
Multifidelity Simulation-based Inference for Computationally Expensive Simulators

Anastasia N. Krouglova^{1,2} Hayden R. Johnson^{1,2} Basile Confavreux³ Michael Deistler^{4,5}
Pedro J. Gonçalves^{1,2,6}

Abstract

Across many domains of science, stochastic models are an essential tool to understand the mechanisms underlying empirically observed data. Models can be of different levels of detail and accuracy, with models of high-fidelity (i.e., high accuracy) to the phenomena under study being often preferable. However, inferring parameters of high-fidelity models via simulation-based inference is challenging, especially when the simulator is computationally expensive. We introduce MF-NPE, a multifidelity approach to neural posterior estimation that leverages inexpensive low-fidelity simulations to infer parameters of high-fidelity simulators within a limited simulation budget. MF-NPE performs neural posterior estimation with limited high-fidelity resources by virtue of transfer learning, with the ability to prioritize individual observations using active learning. On one statistical task with analytical ground-truth and two real-world tasks, MF-NPE shows comparable performance to current approaches while requiring up to two orders of magnitude fewer high-fidelity simulations. Overall, MF-NPE opens new opportunities to perform efficient Bayesian inference on computationally expensive simulators.

1. Introduction

Stochastic models are used across science and engineering to capture complex properties of real systems through simulations (Barbers et al., 2024; Nelson & Pei, 2021; Fadikar

et al., 2018; Pillow & Scott, 2012). These simulators encode domain-specific knowledge and provide a means to generate high-fidelity synthetic data, enabling accurate forward modeling of experimental outcomes. However, inferring model parameters from observed data can be challenging, especially when simulators are stochastic, the likelihoods of the simulators are inaccessible, or when simulations are computationally expensive.

Bayesian inference offers a principled framework to address the challenge of estimating parameters from stochastic observations by quantifying uncertainty in parameter estimates while incorporating prior knowledge. However, classical Bayesian methods are not applicable to cases where the likelihood of the simulator is not accessible in closed form (Tavaré et al., 1997). Simulation-based inference (SBI) has emerged as a paradigm to tackle this by leveraging forward simulations to infer the posterior distribution (Cranmer et al., 2020).

The challenge of extending sampling-based SBI methods like Approximate Bayesian Computation (ABC) (Tavaré et al., 1997; Pritchard et al., 1999) to problems with large numbers of parameters has driven significant advancements (Cranmer et al., 2020). Modern SBI approaches aim for the estimation of the posterior through amortized neural posterior estimation (NPE) (Greenberg et al., 2019; Lueckmann et al., 2017; Papamakarios & Murray, 2016), neural likelihood estimation (Papamakarios et al., 2019), neural ratio estimation (Hermans et al., 2020) and respective sequential variants. These approaches have leveraged recent progress in neural density estimation to improve the scalability and accuracy of SBI, allowing parameter inference in problems with higher dimensionality than was previously achievable (Ramesh et al., 2021; Gloeckler et al., 2024).

Despite these advancements, SBI methods face computational challenges for scenarios involving expensive simulations or high-dimensional parameter spaces, as state-of-the-art methods often require extensive simulation budgets to achieve reliable posterior estimates (Lueckmann et al., 2021).

Multifidelity modeling offers a solution to this problem by

¹Departments of Computer Science and Electrical Engineering, KU Leuven, Belgium ²VIB-Neuroelectronics Research Flanders (NERF), Belgium ³Gatsby Computational Neuroscience Unit, UCL, London, UK ⁴Machine Learning in Science, University of Tübingen, Germany ⁵Tübingen AI Center, Tübingen, Germany ⁶VIB Center for AI & Computational Biology (VIB.AI), Leuven, Belgium. Correspondence to: Anastasia N. Krouglova <nastya.krouglova@nerf.be>, Pedro J. Gonçalves <pedro.goncalves@nerf.be>.

balancing precision and efficiency. It combines accurate but costly high-fidelity models (Hoppe et al., 2021; Behrens & Dias, 2015) with faster, less accurate low-fidelity models. Here, low-fidelity models could be simplifications made possible through domain knowledge about the high-fidelity models, low-dimensional projection of the high-fidelity model, or surrogate modeling (Peherstorfer et al., 2018). For example, Reynolds-averaged Navier-Stokes (RANS) models simplify turbulent flow simulations in aerodynamics (Han et al., 2013), while climate models often reduce complexity by focusing on specific atmospheric effects (Held, 2005; Majda & Gershgorin, 2010). Similarly, mean-field approximations are used to capture certain features of spiking neural network dynamics (Vogels et al., 2011; Dayan & Abbott, 2001). By exploiting this range of fidelities, recent methods in inference, such as multifidelity Monte Carlo approaches (Peherstorfer et al., 2016; Nobile & Tesei, 2015; Giles, 2008; Zeng et al., 2023) have shown clear improvements in computational efficiency through the incorporation of coarse approximations as low-fidelity models. In the context of SBI, we hypothesized that by leveraging the complementarity of high- and low-fidelity simulators, it would be possible to reduce the computational cost of inference while retaining inference accuracy.

In this work, we present MF-NPE, a multifidelity approach that improves the efficiency of amortized neural posterior estimation for expensive simulators. MF-NPE reduces the computational burden of posterior estimation by pre-training a neural density estimator on low-fidelity simulations and refining the inference with a smaller set of high-fidelity simulations. Additionally, we extend our method with active learning, facilitating targeted parameter space exploration to effectively enhance high-fidelity posterior estimates given single observations. We focus on multifidelity cases where both models are simulators and where the low-fidelity model is a simplified version of the high-fidelity model, designed based on domain expertise.

We demonstrate that for one statistical task, with known ground-truth posterior, and two computationally expensive neuroscience simulators, MF-NPE can identify the posterior distributions more efficiently than NPE.

The **core contributions of our work** are:

- A multifidelity approach for NPE. We propose a transfer learning-based method to integrate low- and high-fidelity simulators for efficient posterior estimation of parameters of high-fidelity simulators.
- Sequential multifidelity NPE. We propose two active learning schemes that focus computational resources on the most relevant or informative high-fidelity simulations, further improving computational efficiency.

2. Related work

2.1. Multifidelity methods for inference

Multifidelity has been widely explored in the context of likelihood-based inference (Peherstorfer et al., 2018), from maximum likelihood estimation approaches (Maurais et al., 2023) to Bayesian inference methods (Vo et al., 2019; Catanach et al., 2020).

Currently, few studies tackle the scenario where the likelihood is not explicitly available (Warne et al., 2022; Prescott et al., 2024; Prescott & Baker, 2021). For instance, some multifidelity sampling-based methods have been proposed within the framework of ABC (Prescott & Baker, 2020) or sequential Monte Carlo ABC (Prescott & Baker, 2021). However, despite their potential for multifidelity inference, these methods inherit limitations of ABC approaches, particularly in high-dimensional parameter spaces, where neural density estimators offer more scalable alternatives to complex real-world problems (Lueckmann et al., 2021).

Here, we combine multifidelity approaches with neural density estimation, enabling its application to inference problems with large numbers of model parameters.

2.2. Transfer learning and simulators

To facilitate learning in a target domain, transfer learning borrows knowledge from a source domain (Panigrahi et al., 2021). This is often done when the target dataset is smaller than the source dataset (Larsen-Freeman, 2013) and has successfully been applied to a range of machine learning tasks, e.g., in computer vision (Jiang & Learned-Miller, 2017; Hussain et al., 2019).

In the context of numerical simulators, transfer learning approaches have been used to lower the simulation budget, for instance, in CO₂ forecasting (Falola et al., 2023), surrogate modeling (Wang et al., 2024) and model inversion with physics-informed neural networks (Haghighat et al., 2021). To the best of our knowledge, the potential of transfer learning for computationally-efficient simulation-based inference has not been realized yet.

2.3. Model misspecification

Our work has connections to the issue of model misspecification, a fundamental and widely studied problem in SBI (Gao et al., 2023; Ward et al., 2022; Huang et al., 2023; Frazier et al., 2024; Adachi et al., 2010; Schmitt et al., 2024; Cannon et al., 2022). The issue arises when the probability over the true observation does not fall within the family of estimated probability distributions defined by a model.

A misspecified model can be seen as a form of low-fidelity model of the data-generating process (the high-fidelity

model) since this will often rely on several simplifying assumptions. With this perspective in mind, ROPE can be considered a multifidelity approach to SBI (Wehenkel et al., 2024): model misspecification is addressed by providing a small set of real-world observations that re-calibrate through optimal transport the posterior estimates of the misspecified model. In contrast with our work, this scheme does not allow the active sampling of high-fidelity simulations.

3. Methods

MF-NPE is a multifidelity approach to neural posterior estimation for computationally expensive simulators. We present our approach in Section 3.1. In Section 3.2, we discuss the evaluation metrics used to compare MF-NPE with NPE (Greenberg et al., 2019). MF-NPE is summarized in Algorithm 1 and Fig. 1.

3.1. Multifidelity NPE

We aim to infer the posterior distribution over the parameters θ of a computationally expensive high-fidelity simulator $p(\mathbf{x}|\theta)$, with computational cost c . We designate the simulator as high-fidelity if the model accurately captures the empirical phenomenon, but incurs high computational cost when generating simulations. We assume that we have access to a low-fidelity simulator $p_L(\mathbf{x}_L|\theta)$, describing a simplification of the phenomenon of interest with cost $c_L \ll c$. We assume that both simulators operate over the same domain of observations \mathbf{x} , and the parameters of the low-fidelity model form at least a subset (and at most the entirety) of the high-fidelity parameters. Our goal is to develop an estimator that leverages low-fidelity simulations to infer the posterior distribution over parameters of the high-fidelity model with limited high-fidelity simulations, without access to a tractable likelihood for either simulator.

As with NPE (Papamakarios & Murray, 2016; Greenberg et al., 2019), to estimate the posterior density over model parameters θ for which the likelihood function is unavailable, we consider a sufficiently expressive neural density estimator $q_\phi(\theta|\mathbf{x})$, and train it to minimize the negative log-likelihood loss:

$$\mathcal{L}(\phi) = \mathbb{E}_{\theta \sim p(\theta)} \mathbb{E}_{\mathbf{x} \sim p(\mathbf{x}|\theta)} [-\log q_\phi(\theta|\mathbf{x})], \quad (1)$$

where θ is sampled from the prior distribution and \mathbf{x} denotes the respective simulations (i.e., samples from $p(\mathbf{x}|\theta)$), and ϕ are the network parameters. By minimizing \mathcal{L} , the neural density estimator approximates the conditional distribution $p(\theta|\mathbf{x})$ directly (Papamakarios & Murray, 2016). Given a true observation \mathbf{x}_o , we can then estimate the posterior over parameters $p(\theta|\mathbf{x}_o)$. To ensure $q_\phi(\theta|\mathbf{x}_o)$ closely approximates the true posterior $p(\theta|\mathbf{x}_o)$, the density estimator must be sufficiently expressive. We use neural spline flows (NSF) (Durkan et al., 2019), expressive normalizing flows

that have been shown empirically to be competitive for SBI (Lueckmann et al., 2021).

3.1.1. TRANSFER LEARNING

MF-NPE leverages representations learned from low-fidelity simulations to reduce the number of high-fidelity simulations required to approximate a high-fidelity posterior. To that end, MF-NPE performs *transfer learning*: MF-NPE pre-trains a neural density estimator $q_\psi(\theta|\mathbf{x}_L)$ on low-fidelity simulations, and uses the network parameters ψ as initialization for a high-fidelity density estimator $q_\phi(\theta|\mathbf{x})$. We argue that by pre-training on low-fidelity simulations, the density estimator learns useful features up front – i.e., the feature spaces of the low- and high-fidelity density estimators overlap –, so fewer high-fidelity simulations suffice to refine the posterior estimates. Indeed, Tahir et al. (2024) show that once networks learn suitable features for a given predictive task, they drastically reduce the sample complexity for related tasks. Since we do not freeze the weights after transfer, the network retains the flexibility to adapt to high-fidelity simulations without losing the benefits of pre-training.

We apply MF-NPE to cases where the low-fidelity model has fewer parameters than the high-fidelity model. In this setting, the parameters that are exclusive to the high-fidelity model are treated as dummy variables in the pre-trained density estimator, although it would be possible to further improve this pre-conditioning by adapting the network architecture (Papamakarios et al., 2021). We note that the pre-conditioning with the dummy variables leads to the pre-trained neural density estimator to effectively estimate the prior distribution over the respective parameters (see Appendix B.3). As shown below, MF-NPE shows competitive performance compared to NPE, even when the dimensionality of the low- and high-fidelity model are substantially different (e.g., Section 4.3, where the low- and high-fidelity models have 12 and 14 parameters, respectively).

3.1.2. SEQUENTIAL TRAINING

In addition to learning amortized posterior estimates with NPE, our approach naturally extends to sequential training schemes when estimating the non-amortized posterior $q_\phi(\theta|\mathbf{x}_o)$. Rather than sampling simulation parameters from the prior, sequential methods introduce an active learning scheme that iteratively refines the posterior estimate for a specific observation \mathbf{x}_o .

These methods – known as Sequential Neural Posterior Estimation (Papamakarios & Murray, 2016; Lueckmann et al., 2017) – have shown increased simulation efficiency when compared to NPE (Lueckmann et al., 2021). However, applying these methods with flexible neural density estimators requires a modified loss that suffers from instabilities in training and posterior leakage (Greenberg et al., 2019).

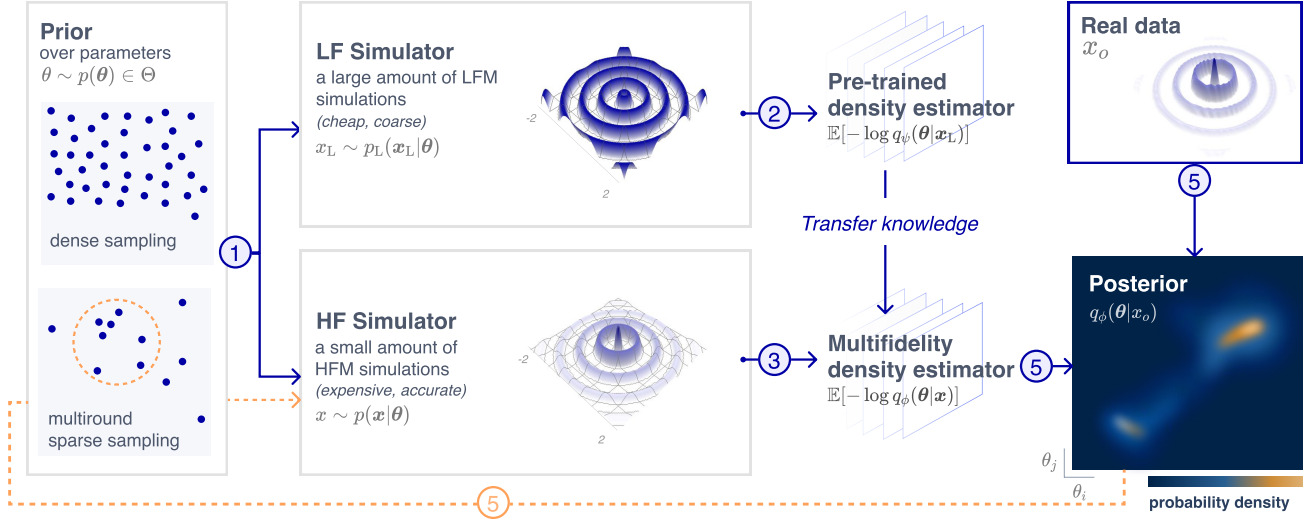


Figure 1. **Multifidelity Neural Posterior Estimation (MF-NPE)**. MF-NPE proceeds by dense sampling from the prior distribution, running the low-fidelity simulator (visualized as a 3D sinusoidal), and training a neural density estimator with a negative log-likelihood loss. MF-NPE then retrains the pre-trained network on sparse samples from the same prior distribution and respective high-fidelity simulations (visualized as a falling waterdrop simulator with exponential decay). Given empirical observations x_o , MF-NPE estimates the posterior distribution given the high-fidelity model. In the sequential case, the parameters for high-fidelity simulations are drawn from iterative refinements of the prior distribution within the support of the current posterior estimate, at some observation x_o .

Truncated Sequential Neural Posterior Estimation (TSNPE) mitigates these issues by sampling from a truncated prior distribution that covers the support of the posterior. This leads to a simplified loss function and increased training stability, while retaining performance (Deistler et al., 2022).

We apply our multifidelity approach to TSNPE. First, the high-fidelity density estimator is initialized from the learned network parameters of a low-fidelity density estimator. Then, high-fidelity simulations are generated iteratively from a truncated prior, within the support of the current posterior. We refer to this method as MF-TSNPE (complete description of the algorithm in Appendix F.1).

3.1.3. ACQUISITION FUNCTION

To further enhance the efficiency of our sequential algorithm, we explore the use of an acquisition function to supplement our round-wise samples from the TSNPE proposal. In particular, we generate simulations for round i with a set of parameters $\theta^{(i)} = \{\theta_{\text{prop}}^{(i)} \cup \theta_{\text{active}}^{(i)}\}$ where $\theta_{\text{prop}}^{(i)}$ are samples from the the proposal distribution at round i , and $\theta_{\text{active}}^{(i)}$ are the top B values according to an acquisition function.

Following Järvenpää et al. (2019); Lueckmann et al. (2019), we select an acquisition function that targets the variance of the posterior estimate with respect to the uncertainty in the

learned parameters $\phi|\mathcal{D}$.

$$\theta^* = \operatorname{argmax}_{\theta} \nabla_{\phi|\mathcal{D}} [q_{\phi}(\theta|x_o)] \quad (2)$$

We realize this as the sample variance across an ensemble of neural density estimators trained independently on the same dataset \mathcal{D} — as done in Lueckmann et al. (2019). Alternatively, one could estimate $\phi|\mathcal{D}$ using other methods of uncertainty quantification such as Monte Carlo dropout as demonstrated in Griesemer et al. (2024).

The addition of an acquisition function raises the possibility of biasing the proposal distribution, causing the density estimate to diverge from the true posterior. In principle, this could be addressed by using atomic proposals (Greenberg et al., 2019), but given that such an approach suffers from posterior leakage, we do not introduce a proposal correction in order to retain the well-behaved loss function in TSNPE. We hypothesized that the benefit of informative samples would outweigh the potential bias, as long as the percentage of samples selected from the acquisition function would be small compared to the proposal samples, and indeed, our empirical results support this. We refer to this algorithm as A-MF-TSNPE (full description in Appendix F.2).

3.2. Evaluation metrics

We evaluate the method on observations x_o from the high-fidelity simulator, with parameter values drawn from the

Algorithm 1 MF-NPE

Input: N pairs of (θ, \mathbf{x}_L) ; M pairs of (θ, \mathbf{x}) ; conditional density estimators $q_\psi(\theta|\mathbf{x}_L)$ and $q_\phi(\theta|\mathbf{x})$ with respectively learnable parameters ψ and ϕ ; early stopping criterion S .

$$\mathcal{L}(\psi) = \frac{1}{N} \sum_{i=1}^N -\log q_\psi(\theta_i|\mathbf{x}_i^L).$$

for epoch in epochs **do**

 train q_ψ to minimize $\mathcal{L}(\psi)$ until S is reached.

end for

Initialize q_ϕ with weights and biases of trained q_ψ .

$$\mathcal{L}(\phi) = \frac{1}{M} \sum_{i=1}^M -\log q_\phi(\theta_i|\mathbf{x}_i).$$

for epoch in epochs **do**

 train q_ϕ to minimize $\mathcal{L}(\phi)$ until S is reached.

end for

prior distribution. This ensured a fair evaluation of how much the low-fidelity simulator helps to infer the posterior distribution given the high-fidelity model.

All methods were evaluated for a range of high-fidelity simulation budgets ($50, 10^2, 10^3, 10^4, 10^5$), on posteriors given the same data set of observations x_o .

Known true posterior We evaluate the method with the Classifier-2-Sample Test (C2ST) (Friedman, 2004; Lopez-Paz & Oquab, 2017), which allows evaluating the accuracy of posterior distributions in cases when the ground-truth posterior is known (Lueckmann et al., 2021). Here, a value close to 0.5 means that a classifier does not effectively distinguish the two distributions, and therefore, the posterior estimate is close to the ground-truth posterior. A value close to 1 means that the classifier can distinguish the distributions very well, indicating a poor posterior estimation. This framework is not applicable in most practical SBI settings, since it requires samples from the true posterior and is primarily used in toy examples (e.g., Section 4.1).

Unknown true posterior The average Negative Log probability of the True Parameters (NLTP; $-\mathbb{E}[\log q(\theta_o|\mathbf{x}_o)]$) is a commonly reported metric in simulation-based inference for problems where the true posterior is unknown (Greenberg et al., 2019; Papamakarios & Murray, 2016; Durkan et al., 2020). In the limit of a large number of pairs (θ_o, \mathbf{x}_o) , the average over the log probability of each pair (θ_o, \mathbf{x}_o) approaches the expected KL divergence between the estimated and the true posterior (up to a term that is independent of the estimated posterior), as shown in (Lueckmann et al., 2021).

4. Results

We evaluate the performance of our multifidelity approach to simulation-based inference on three tasks. We start with the Ornstein-Uhlenbeck process, for which the likelihood

function is available in closed form, and follow with two challenging neuroscience problems with computationally expensive simulators and for which no likelihood is available: a multicompartmental neuron model, and a neural network model with synaptic plasticity.

4.1. Ornstein-Uhlenbeck process

Consider a drift-diffusion process of a particle starting at position $X(0)$ and drifting towards an equilibrium state. In this task, the Ornstein-Uhlenbeck (OU) process is the high-fidelity model of this phenomenon and has four parameters: the long-term mean μ , volatility σ , rate of mean reversion γ , and μ_{offset} , which is the distance between the initial position $X(0)$ and μ . As low-fidelity model, we chose i.i.d. samples from a Gaussian distribution, parametrized by μ_L and σ_L (Fig. 2; Appendix B for details).

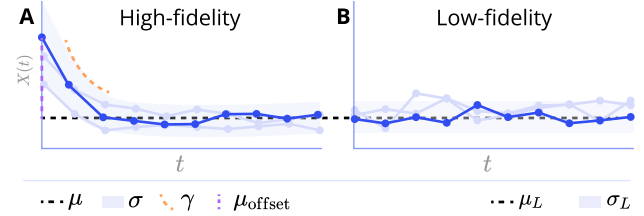


Figure 2. (A) **High-fidelity model:** Time-dependent Ornstein-Uhlenbeck process with four parameters. (B) **Low-fidelity model:** Time-independent i.i.d. Gaussian samples with two parameters.

The Ornstein-Uhlenbeck (OU) process has a tractable likelihood, which is given by

$$p_{\text{exact}}(\mathbf{X} | \mu, \sigma, \gamma, \mu_{\text{offset}}) = p(X(0)) \prod_{t=1}^n \frac{1}{\sqrt{\pi}g\sigma} \exp^{K_t}, \quad (3)$$

where K is defined as

$$K_t = -\frac{1}{g\sigma^2} \left((\mu - X_t) - \sqrt{1 - \gamma g} (\mu - X_{t-1}) \right)^2,$$

$p(X(0)) = \mathcal{N}(\mu + \mu_{\text{offset}}, 1)$ is the distribution over initial conditions, and $g = (1 - \exp(-2\gamma\Delta T))/\gamma$ (details in Appendix B.1) (Kou et al., 2012).

To evaluate MF-NPE, we compared the estimated densities to the respective reference posterior, estimated from the exact likelihood with rejection sampling (Martino et al., 2018). We quantified the performance with the Classifier-2-Sample Test (C2ST) over 30 observations and 10 network initializations per observation.

First, we evaluated our multifidelity approach in a setting where the low- and high-fidelity models have the same number of parameters (Fig. 3). Second, we gradually increased the number of parameters of the high-fidelity model by

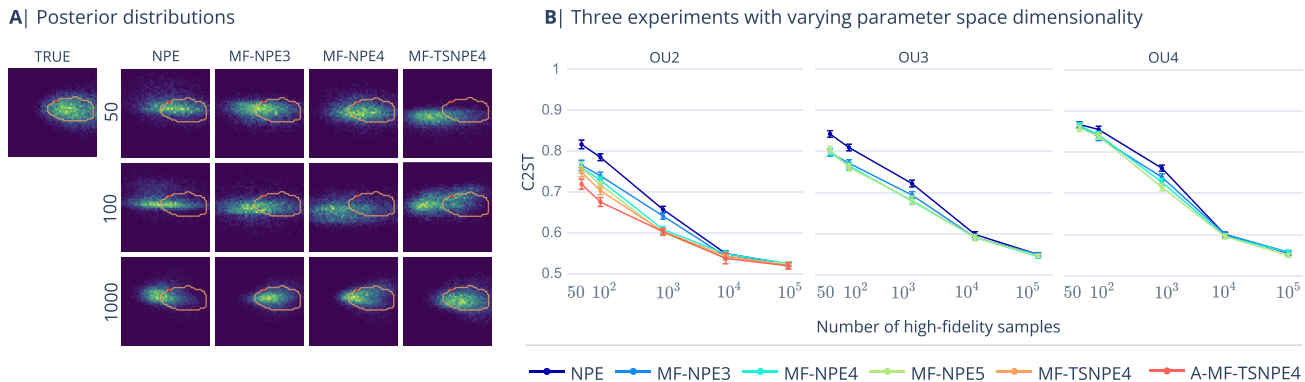


Figure 3. MF-NPE is sample efficient. (A) Posterior density estimates for a single observation from the OU process with two free parameters (OU2). The orange contour lines contain 68% of the probability mass of the true posterior distribution. (B) C2ST averaged over 10 network initializations: means and 95% confidence intervals. MF-NPE3 is pre-trained on a low-fidelity dataset of size 10^3 , while MF-NPE4 and MF-NPE5 use datasets of 10^4 and 10^5 low-fidelity simulations, respectively. MF-NPE improves its performance with a larger number of low-fidelity samples, and all variants of our method perform better than NPE.

adding the mean reversion γ and μ_{offset} , resulting in a setup with three and four parameters for the high-fidelity model versus two for the low-fidelity model. We designate the three experiments OU2, OU3 and OU4, respectively.

Across experiments, we observed a consistent increase in performance with MF-NPE compared to NPE, especially in low simulation budgets from the high-fidelity model (50-1000 simulations) (Fig. 3). In addition, we found that having a higher number of low-fidelity samples improved performance, reinforcing that low-fidelity simulations were indeed advantageous for pre-training the neural density estimator for the downstream task. Note that in this task, we did not observe a substantial increase in MF-NPE performance between the setting with 10^4 and 10^5 low-fidelity samples, suggesting that we might have reached an upper bound regarding pre-training efficacy.

We expected that adding parameters to the high-fidelity model that are not present in the low-fidelity model, increased the complexity of the inference problem for MF-NPE, and indeed observed a decrease in MF-NPE performance, although MF-NPE still performed better than NPE.

As described in Section 3, we enhanced the sequential algorithm TSNPE (Deistler et al., 2022) with a first round of MF-NPE, and designated this approach as MF-TSNPE. We found that MF-TSNPE (with 5 rounds; more details in Appendix F.1) performs better than the amortized MF-NPE, especially in regimes with low budget of high-fidelity simulations, further confirming previous findings that sequential methods have substantially higher performance in non-amortized scenarios (Lueckmann et al., 2021).

Finally, we found that A-MF-TSNPE shows minor improvements compared to MF-TSNPE. Such an approach is substantially more costly to run (given the ensemble of density

estimators) and has a larger number of hyperparameters to tune. We cannot exclude the hypothesis that larger performance gains could be obtained from such an approach by a more extensive hyperparameter search.

Overall, the results of the Ornstein-Uhlenbeck task suggest that MF-NPE and MF-TSNPE have the potential to lead to substantial performance gains compared to NPE.

4.2. Multicompartmental neuron model

The voltage response of a morphologically-detailed neuron to an input current is typically modeled with a multicompartment model wherein the voltage dynamics of each compartment are based on the Hodgkin-Huxley equations (Hodgkin & Huxley, 1952; Hay et al., 2011; Druckmann et al., 2007). The higher the number of compartments of the model, the more accurate the model is, but the higher the simulation cost.

In this task, we aimed to infer the densities of ion channels \bar{g}_{Na} and \bar{g}_K on a morphologically-detailed model of a thick-tufted layer 5 pyramidal cell (L5PC) containing 8 compartments per branch (Fig. 4A) (Van Geit et al., 2016). We injected in the first neuron compartment a noisy 100 ms step current with mean $I_m = 0.3$ nA: $I_e = I_m + \epsilon$, $\epsilon \sim \mathcal{N}(0, 0.01)$. The voltage response of the neuron was recorded over 120 ms, with a simulation step size of 0.025 ms and 10 ms margin before and after the current injection. We defined the high-fidelity model to have 8 compartments per branch and the low-fidelity model to have 1 compartment per branch, and both the high and low-fidelity models had the same injected current and ion channel types.

To simulate the neuron models, we used Jaxley, a Python toolbox that makes use of GPU acceleration for efficiently simulating multicompartment single neurons with biophys-

ical detail (Deistler et al., 2024). In this setting, the simulation time for the high-fidelity model is approximately 7 times higher than that of the low-fidelity model.

We characterized the neural response with four summary statistics that have been commonly used when fitting biophysical models of single neurons to empirical data: number of spikes, mean resting potential, standard deviation of the resting potential, and the voltage mean (Gonçalves et al., 2020; Gao et al., 2023).

The performances of MF-NPE and NPE were evaluated with NLTP on 10^3 pairs of θ_o and respective simulation outputs x_o (see Section 3.2), averaged over 10 different random network initialization and fixed simulation data set.

In line with the results in the OU process task, MF-NPE showed much better performance than NPE in terms of NLTP, in particular with higher low-fidelity simulation budgets (Fig. 4B,C). Furthermore, posterior predictives of MF-NPE closely matched the empirical data, in contrast with NPE, even when NPE was trained on a higher number of high-fidelity simulations (Fig. 4D; Appendix C). Finally, we ran simulation-based calibration tests and found that both MF-NPE and NPE estimates are relatively well calibrated (Fig. 4E) (Talts et al., 2020).

4.3. Recurrent Spiking Network

Finally, we applied MF-NPE to a particularly challenging and timely problem in neuroscience: the inference of synaptic plasticity rules that endow large spiking neural networks with dynamics reminiscent of experimental data. This problem has been recently tackled with an SBI method (filter simulation-based inference, fSBI) that progressively narrows down the search space of parameters given different sets of summary statistics (Confavreux et al., 2023). fSBI was successful in obtaining manifolds of plasticity rules that ensure plausible network activity, but the compute requirements were reported to be very large. Here, we aim to test whether this problem can be efficiently tackled with MF-NPE.

The high-fidelity simulator consisted of a recurrent network of 4096 excitatory (E) and 1024 inhibitory (I) leaky integrate-and-fire neurons connected with conductance-based synapses (Fig. 5A, B). Each synapse type in this network (E -to- E , E -to- I , I -to- E and I -to- I) was plastic with an unsupervised local learning rule. For each synapse type, six parameters governed how the recent pre- and post-synaptic activity were used to update the synapse, for a total of 24 free parameters across all 4 synapse types, following previous work (Confavreux et al., 2023). The networks were simulated using Auryn, a C++ simulator (Zenke & Gerstner, 2014) (additional details in Appendix D).

Mean-field theory can be applied to the dynamical system

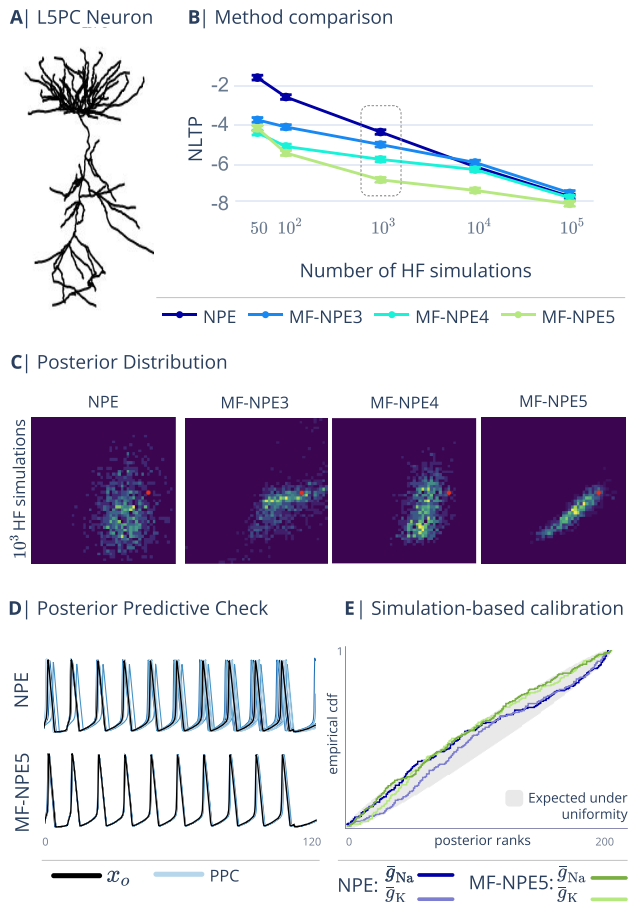


Figure 4. (A) A thick-tufted layer 5 pyramidal cell from the neocortex, containing 1 or 8 compartments per branch, respectively for the low- and high-fidelity models. (B) NLTP evaluated on 1000 pairs of observations and respective true parameters. Different colors of MF-NPE correspond to different numbers of low-fidelity samples used to pre-train the model (respectively 10^3 , 10^4 , 10^5 ; same naming convention as in Fig. 3). (C) Posterior distributions across 4 methods, trained on 10^3 high-fidelity samples (dotted box in panel B). (D) Posterior predictives, where NPE and MF-NPE have been trained on 10^3 high-fidelity samples. (E) Simulation-based calibration for NPE and MF-NPE trained on 10^3 samples.

above to obtain the steady-state activities of the excitatory and inhibitory populations as a function of the parameters of the plasticity rules embedded in the network. Though such analysis is widely performed in the field (Vogels et al., 2011; Confavreux et al., 2023; Gerstner & Kistler, 2002; Gerstner et al., 2014), it has never been used as a low-fidelity model to help with the inference of the high-fidelity model parameters (additional details in Appendix D). Since there are no dynamics to simulate with the mean-field model, the simulation was almost instantaneous, while the high-fidelity model took approximately 5 minutes to generate a 2-minute long simulation on a single CPU.

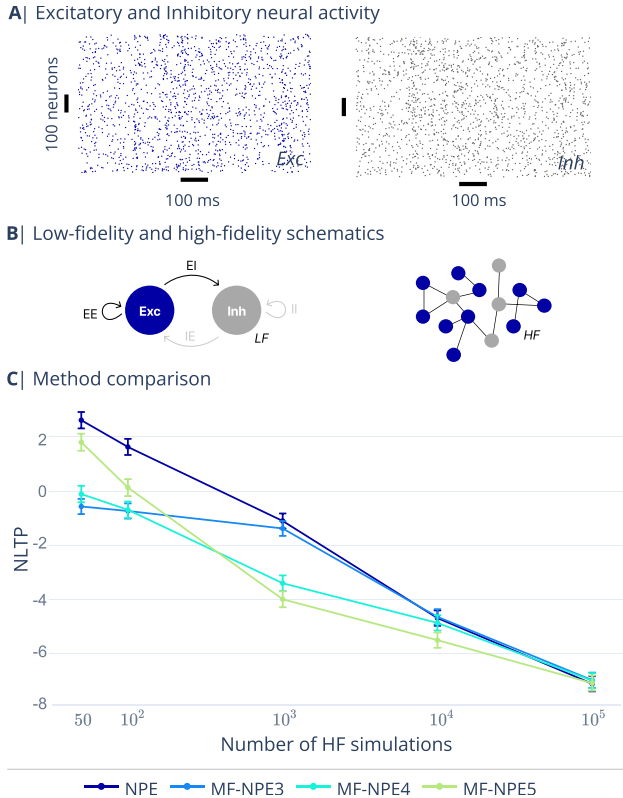


Figure 5. (A) Example raster plots of the neural activities in a recurrent plastic network over 1s time window. (B) Schematics of the low- and high-fidelity models of a spiking network. (C) Performance of NPE and MF-NPE evaluated on 1000 true observations with NLTP, and averaged over 10 network initializations, with 95% confidence intervals.

Summary statistics for both the low- and high-fidelity models were two-dimensional: the average firing rates of the excitatory and inhibitory neurons at steady state (after 2 minutes of simulation in the high-fidelity model). Plastic networks were considered plausible if the measured firing rates were between 1 and 50Hz (Dayan & Abbott, 2001; Confavreux et al., 2023).

Note that in our task, the low-fidelity model focuses solely on the E -to- E and E -to- I rules from the high-fidelity model, thereby having 12 out of the 24 parameters of the high-fidelity model. This setup allows us to demonstrate the performance of MF-NPE on problems with different parameter spaces, highlighting MF-NPE’s flexibility and advantages.

We found that MF-NPE has better performance than NPE in terms of NLTP (Fig. 5C). Furthermore, MF-NPE leads to an increase of almost 30% in the proportion of posterior samples within the target firing rate bounds (Table 1), reinforcing that MF-NPE is a practical and effective method for simulation-based inference of costly real-world simulators.

Table 1. Comparison between methods. MF-NPE4 is pretrained on 10^4 low-fidelity samples, and MF-NPE5 on 10^5 samples.

Method	# simulations	rates 1–50 Hz
NPE	HF: 10^3	66.4%
MF-NPE4	HF: 10^3 ; LF: 10^4	94.2%
MF-NPE5	HF: 10^3 ; LF: 10^5	95.6%

5. Discussion

We proposed a new method for simulation-based inference that leverages low-fidelity models to efficiently infer the parameters of costly high-fidelity models. By incorporating transfer learning and multifidelity approaches, MF-NPE substantially reduces the simulation budget required for accurate posterior inference. This addresses a pervasive challenge across scientific domains: the high computational cost of simulating complex high-fidelity models and linking them to empirical data. Our empirical results demonstrate MF-NPE’s competitive performance in SBI across statistical benchmarks and real-world applications, as compared to a standard method such as NPE.

Despite MF-NPE’s advantages, the method comes with some challenges. First, the effectiveness of MF-NPE relies on the similarity between the low-fidelity and high-fidelity models. Fortunately, in many situations, domain experts will know beforehand whether low-fidelity models are poor approximations of high-fidelity models. Second, MF-NPE and MF-TSNPE inherit the limitations of NPE and TSNPE, respectively, in particular regarding the scalability of simulation-based inference to high-dimensional parameter spaces. How to balance exploration of high-dimensional parameter spaces and computational cost in a simulation-based inference setting remains a topic of active research.

We identify two promising research directions in the realm of multifidelity simulation-based inference. First, we expect that the scalability and expressivity of MF-NPE can be improved by utilizing the same approaches of multifidelity and transfer learning presented here with neural density estimators other than normalizing flows, such as diffusion models (Gloeckler et al., 2024). Second, similar to past efforts in developing a benchmark for simulation-based inference, it will be beneficial for the SBI community to develop a benchmark for multifidelity problems, with new tasks, algorithms and evaluation metrics. This will promote rigorous and reproducible research and catalize new developments in multifidelity SBI, and in SBI more generally. Our work and codebase are a step in this direction.

Conclusion Overall, MF-NPE is a method for simulation-based inference that leverages low-fidelity models and transfer learning to infer the parameters of costly high-fidelity

models, thus providing an effective balance between computational cost and inference accuracy.

Impact Statement

This paper presents work whose goal is to advance the field of Machine Learning. There are many potential societal consequences of our work, none which we feel must be specifically highlighted here.

References

- Adachi, T., Kunitomo, H., Tomioka, M., Ohno, H., Okochi, Y., Mori, I., and Iino, Y. Reversal of Salt Preference Is Directed by the Insulin/PI3K and Gq/PKC Signaling in *Caenorhabditis elegans*. *Genetics*, 186(4):1309–1319, December 2010. ISSN 0016-6731. doi: 10.1534/genetics.110.119768.
- Barbers, E., Hust, F. E., Hildenbrand, F. E. A., Frie, F., Quade, K. L., Bihn, S., Sauer, D. U., and Dechent, P. Exploring the effects of cell-to-cell variability on battery aging through stochastic simulation techniques. *Journal of Energy Storage*, 84:110851, April 2024. ISSN 2352-152X. doi: 10.1016/j.est.2024.110851.
- Behrens, J. and Dias, F. New computational methods in tsunami science. *Philosophical Transactions of the Royal Society A: Mathematical, Physical and Engineering Sciences*, 373(2053):20140382, October 2015. doi: 10.1098/rsta.2014.0382.
- Boelts, J., Deistler, M., Gloeckler, M., Tejero-Cantero, A., Lueckmann, J.-M., Moss, G., Steinbach, P., Moreau, T., Muratore, F., Linhart, J., Durkan, C., Vetter, J., Miller, B. K., Herold, M., Ziaemehr, A., Pals, M., Gruner, T., Bischoff, S., Krouglova, N., Gao, R., Lappalainen, J. K., Mucsányi, B., Pei, F., Schulz, A., Stefanidi, Z., Rodrigues, P., Schröder, C., Zaid, F. A., Beck, J., Kapoor, J., Greenberg, D. S., Gonçalves, P. J., and Macke, J. H. sbi reloaded: a toolkit for simulation-based inference workflows, November 2024.
- Cannon, P., Ward, D., and Schmon, S. M. Investigating the Impact of Model Misspecification in Neural Simulation-based Inference, September 2022.
- Catanach, T. A., Vo, H. D., and Munsky, B. Bayesian inference of stochastic reaction networks using multifidelity sequential tempered Markov Chain Monte Carlo. *International Journal for Uncertainty Quantification*, 10(6): 515–542, 2020. ISSN 2152-5080. doi: 10.1615/int.j.uncertaintyquantification.2020033241.
- Confavreux, B., Ramesh, P., Gonçalves, P. J., Macke, J. H., and Vogels, T. Meta-learning families of plasticity rules in recurrent spiking networks using simulation-based inference. *Advances in Neural Information Processing Systems*, 36:13545–13558, December 2023.
- Cranmer, K., Brehmer, J., and Louppe, G. The frontier of simulation-based inference. *Proceedings of the National Academy of Sciences*, 117(48):30055–30062, December 2020. doi: 10.1073/pnas.1912789117.
- Dayan, P. and Abbott, L. F. *Theoretical neuroscience: computational and mathematical modeling of neural systems*. Computational neuroscience. Massachusetts Institute of Technology Press, Cambridge, Mass, 2001. ISBN 978-0-262-04199-7.
- Deistler, M., Gonçalves, P. J., and Macke, J. H. Truncated proposals for scalable and hassle-free simulation-based inference. *Advances in Neural Information Processing Systems*, 35:23135–23149, December 2022.
- Deistler, M., Kadhim, K. L., Pals, M., Beck, J., Huang, Z., Gloeckler, M., Lappalainen, J. K., Schröder, C., Berens, P., Gonçalves, P. J., and Macke, J. H. Differentiable simulation enables large-scale training of detailed biophysical models of neural dynamics, August 2024.
- Druckmann, S., Banitt, Y., Gidon, A., Schürmann, F., Markram, H., and Segev, I. A novel multiple objective optimization framework for constraining conductance-based neuron models by experimental data. *Frontiers in Neuroscience*, 1, 2007. ISSN 1662-453X.
- Durkan, C., Bekasov, A., Murray, I., and Papamakarios, G. Neural Spline Flows. In *Advances in Neural Information Processing Systems*, volume 32. Curran Associates, Inc., 2019.
- Durkan, C., Murray, I., and Papamakarios, G. On Contrastive Learning for Likelihood-free Inference. In *Proceedings of the 37th International Conference on Machine Learning*, pp. 2771–2781. PMLR, November 2020.
- Fadikar, A., Higdon, D., Chen, J., Lewis, B., Venkatraman, S., and Marathe, M. Calibrating a Stochastic, Agent-Based Model Using Quantile-Based Emulation. *SIAM/ASA Journal on Uncertainty Quantification*, 6(4): 1685–1706, January 2018. doi: 10.1137/17M1161233.
- Falola, Y., Misra, S., and Nunez, A. C. Rapid High-Fidelity Forecasting for Geological Carbon Storage Using Neural Operator and Transfer Learning. In *ADIPEC*, Abu Dhabi, UAE, October 2023. OnePetro. doi: 10.2118/216135-MS.
- Frazier, D. T., Nott, D. J., and Drovandi, C. Synthetic Likelihood in Misspecified Models. *Journal of the American Statistical Association*, 0(0):1–12, 2024. ISSN 0162-1459. doi: 10.1080/01621459.2024.2370594.

- Friedman, J. On Multivariate Goodness-of-Fit and Two-Sample Testing. Technical Report SLAC-PUB-10325, 826696, Stanford, January 2004.
- Gao, R., Deistler, M., and Macke, J. H. Generalized Bayesian Inference for Scientific Simulators via Amortized Cost Estimation, November 2023.
- Gerstner, W. and Kistler, W. M. Mathematical formulations of Hebbian learning. *Biological Cybernetics*, 87(5):404–415, December 2002. ISSN 1432-0770. doi: 10.1007/s00422-002-0353-y.
- Gerstner, W., Kistler, W. M., Naud, R., and Paninski, L. *Neuronal Dynamics: From Single Neurons to Networks and Models of Cognition*. Cambridge University Press, Cambridge, 2014. ISBN 978-1-107-06083-8. doi: 10.1017/CBO9781107447615.
- Giles, M. B. Multilevel Monte Carlo Path Simulation. *Operations Research*, 56(3):607–617, June 2008. ISSN 0030-364X. doi: 10.1287/opre.1070.0496.
- Gloeckler, M., Deistler, M., Weilbach, C., Wood, F., and Macke, J. H. All-in-one simulation-based inference, May 2024.
- Gonçalves, P. J., Lueckmann, J.-M., Deistler, M., Nonnenmacher, M., Öcal, K., Bassetto, G., Chintaluri, C., Podlaski, W. F., Haddad, S. A., Vogels, T. P., Greenberg, D. S., and Macke, J. H. Training deep neural density estimators to identify mechanistic models of neural dynamics. *eLife*, 9:e56261, September 2020. ISSN 2050-084X. doi: 10.7554/eLife.56261.
- Greenberg, D., Nonnenmacher, M., and Macke, J. Automatic Posterior Transformation for Likelihood-Free Inference. In *Proceedings of the 36th International Conference on Machine Learning*, pp. 2404–2414. PMLR, May 2019.
- Griesemer, S., Cao, D., Cui, Z., Osorio, C., and Liu, Y. Active Sequential Posterior Estimation for Sample-Efficient Simulation-Based Inference. In *Neural Information Processing Systems*, November 2024.
- Haghighat, E., Raissi, M., Moure, A., Gomez, H., and Juanes, R. A physics-informed deep learning framework for inversion and surrogate modeling in solid mechanics. *Computer Methods in Applied Mechanics and Engineering*, 379:113741, June 2021. ISSN 0045-7825. doi: 10.1016/j.cma.2021.113741.
- Han, Z.-H., Görtz, S., and Zimmermann, R. Improving variable-fidelity surrogate modeling via gradient-enhanced kriging and a generalized hybrid bridge function. *Aerospace Science and Technology*, 25(1):177–189, March 2013. ISSN 1270-9638. doi: 10.1016/j.ast.2012.01.006.
- Hay, E., Hill, S., Schürmann, F., Markram, H., and Segev, I. Models of neocortical layer 5b pyramidal cells capturing a wide range of dendritic and perisomatic active properties. *PLoS computational biology*, 7(7):e1002107, July 2011. ISSN 1553-7358. doi: 10.1371/journal.pcbi.1002107.
- Held, I. M. The Gap between Simulation and Understanding in Climate Modeling. *ametsoc*, November 2005. doi: 10.1175/BAMS-86-11-1609.
- Hermans, J., Begy, V., and Louppe, G. Likelihood-free MCMC with Amortized Approximate Ratio Estimators. In *Proceedings of the 37th International Conference on Machine Learning*, pp. 4239–4248. PMLR, November 2020.
- Hodgkin, A. L. and Huxley, A. F. A quantitative description of membrane current and its application to conduction and excitation in nerve. *The Journal of Physiology*, 117(4):500–544, August 1952. ISSN 0022-3751.
- Hoppe, M., Embreus, O., and Fülöp, T. DREAM: A fluid-kinetic framework for tokamak disruption runaway electron simulations. *Computer Physics Communications*, 268:108098, November 2021. ISSN 0010-4655. doi: 10.1016/j.cpc.2021.108098.
- Huang, D., Bharti, A., Souza, A., Acerbi, L., and Kaski, S. Learning Robust Statistics for Simulation-based Inference under Model Misspecification. *Advances in Neural Information Processing Systems*, 36:7289–7310, December 2023.
- Hussain, M., Bird, J. J., and Faria, D. R. A Study on CNN Transfer Learning for Image Classification. In Lotfi, A., Bouchachia, H., Gegov, A., Langensiepen, C., and McGinnity, M. (eds.), *Advances in Computational Intelligence Systems*, pp. 191–202, Cham, 2019. Springer International Publishing. ISBN 978-3-319-97982-3. doi: 10.1007/978-3-319-97982-3_16.
- Jiang, H. and Learned-Miller, E. Face Detection with the Faster R-CNN. In *2017 12th IEEE International Conference on Automatic Face & Gesture Recognition (FG 2017)*, pp. 650–657, May 2017. doi: 10.1109/FG.2017.82.
- Järvenpää, M., Gutmann, M. U., Pleska, A., Vehtari, A., and Martinen, P. Efficient Acquisition Rules for Model-Based Approximate Bayesian Computation. *Bayesian Analysis*, 14(2):595–622, June 2019. ISSN 1936-0975, 1931-6690. doi: 10.1214/18-BA1121.
- Kou, S., Olding, B., Lysy, M., and Liu, J. A Multiresolution Method for Parameter Estimation of Diffusion Processes. *Journal of The American Statistical Association - J AMER STATIST ASSN*, 107:4, December 2012. doi: 10.1080/01621459.2012.720899.

- Larsen-Freeman, D. Transfer of Learning Transformed. *Language Learning*, 63(s1):107–129, 2013. ISSN 1467-9922. doi: 10.1111/j.1467-9922.2012.00740.x.
- Lopez-Paz, D. and Oquab, M. Revisiting Classifier Two-Sample Tests. In *International Conference on Learning Representations*, Toulon, France, 2017. International Conference on Learning Representations. doi: 10.48550/arXiv.1610.06545.
- Lueckmann, J.-M., Goncalves, P. J., Bassetto, G., Öcal, K., Nonnenmacher, M., and Macke, J. H. Flexible statistical inference for mechanistic models of neural dynamics. In *Advances in Neural Information Processing Systems*, volume 30. Curran Associates, Inc., 2017.
- Lueckmann, J.-M., Bassetto, G., Karaletsos, T., and Macke, J. H. Likelihood-free inference with emulator networks. In *Proceedings of The 1st Symposium on Advances in Approximate Bayesian Inference*, pp. 32–53. PMLR, January 2019.
- Lueckmann, J.-M., Boelts, J., Greenberg, D., Goncalves, P., and Macke, J. Benchmarking Simulation-Based Inference. In *Proceedings of The 24th International Conference on Artificial Intelligence and Statistics*, pp. 343–351. PMLR, March 2021.
- Majda, A. J. and Gershgorin, B. Quantifying uncertainty in climate change science through empirical information theory. *Proceedings of the National Academy of Sciences of the United States of America*, 107(34):14958–14963, 2010. ISSN 0027-8424.
- Martino, L., Luengo, D., and Míguez, J. Accept–Reject Methods. In Martino, L., Luengo, D., and Míguez, J. (eds.), *Independent Random Sampling Methods*, pp. 65–113. Springer International Publishing, Cham, 2018. ISBN 978-3-319-72634-2. doi: 10.1007/978-3-319-72634-2_3.
- Maurais, A., Alsup, T., Peherstorfer, B., and Marzouk, Y. Multifidelity Covariance Estimation via Regression on the Manifold of Symmetric Positive Definite Matrices. *SIAM Journal on Scientific Computing*, 2023. doi: 10.48550/ARXIV.2307.12438.
- Nelson, B. L. and Pei, L. *Foundations and Methods of Stochastic Simulation: A First Course*, volume 316 of *International Series in Operations Research & Management Science*. Springer International Publishing, Cham, 2021. ISBN 978-3-030-86193-3 978-3-030-86194-0. doi: 10.1007/978-3-030-86194-0.
- Nobile, F. and Tesei, F. A Multi Level Monte Carlo method with control variate for elliptic PDEs with log-normal coefficients. *Stochastic Partial Differential Equations: Analysis and Computations*, 3(3):398–444, September 2015. ISSN 2194-041X. doi: 10.1007/s40072-015-0055-9.
- Panigrahi, S., Nanda, A., and Swarnkar, T. A Survey on Transfer Learning. In Mishra, D., Buyya, R., Mohapatra, P., and Patnaik, S. (eds.), *Intelligent and Cloud Computing*, pp. 781–789, Singapore, 2021. Springer. ISBN 9789811559716. doi: 10.1007/978-981-15-5971-6_83.
- Papamakarios, G. and Murray, I. Fast ϵ -free Inference of Simulation Models with Bayesian Conditional Density Estimation. In *Advances in Neural Information Processing Systems*, volume 29. Curran Associates, Inc., 2016.
- Papamakarios, G., Sterratt, D., and Murray, I. Sequential Neural Likelihood: Fast Likelihood-free Inference with Autoregressive Flows. In *Proceedings of the Twenty-Second International Conference on Artificial Intelligence and Statistics*, pp. 837–848. PMLR, April 2019.
- Papamakarios, G., Nalisnick, E., Rezende, D. J., Mohamed, S., and Lakshminarayanan, B. Normalizing Flows for Probabilistic Modeling and Inference. *Journal of Machine Learning Research*, 22(57):1–64, 2021. ISSN 1533-7928.
- Paszke, A., Gross, S., Massa, F., Lerer, A., Bradbury, J., Chanan, G., Killeen, T., Lin, Z., Gimelshein, N., Antiga, L., Desmaison, A., Kopf, A., Yang, E., DeVito, Z., Raison, M., Tejani, A., Chilamkurthy, S., Steiner, B., Fang, L., Bai, J., and Chintala, S. PyTorch: An Imperative Style, High-Performance Deep Learning Library. In *Advances in Neural Information Processing Systems*, volume 32. Curran Associates, Inc., 2019.
- Peherstorfer, B., Willcox, K., and Gunzburger, M. Optimal Model Management for Multifidelity Monte Carlo Estimation. *SIAM Journal on Scientific Computing*, 38(5):A3163–A3194, January 2016. ISSN 1064-8275. doi: 10.1137/15M1046472.
- Peherstorfer, B., Willcox, K., and Gunzburger, M. Survey of Multifidelity Methods in Uncertainty Propagation, Inference, and Optimization. *SIAM Review*, 60(3):550–591, January 2018. ISSN 0036-1445. doi: 10.1137/16M1082469.
- Pillow, J. and Scott, J. Fully Bayesian inference for neural models with negative-binomial spiking. In *Advances in Neural Information Processing Systems*, volume 25. Curran Associates, Inc., 2012.
- Prescott, T. P. and Baker, R. E. Multifidelity Approximate Bayesian Computation. *SIAM/ASA Journal on Uncertainty Quantification*, 8(1):114–138, January 2020. doi: 10.1137/18M1229742.

- Prescott, T. P. and Baker, R. E. Multifidelity Approximate Bayesian Computation with Sequential Monte Carlo Parameter Sampling. *SIAM/ASA Journal on Uncertainty Quantification*, 9(2):788–817, January 2021. doi: 10.1137/20M1316160.
- Prescott, T. P., Warne, D. J., and Baker, R. E. Efficient multifidelity likelihood-free Bayesian inference with adaptive computational resource allocation. *Journal of Computational Physics*, 496:112577, January 2024. ISSN 0021-9991. doi: 10.1016/j.jcp.2023.112577.
- Pritchard, J. K., Seielstad, M. T., Perez-Lezaun, A., and Feldman, M. W. Population growth of human Y chromosomes: a study of Y chromosome microsatellites. *Molecular Biology and Evolution*, 16(12):1791–1798, December 1999. ISSN 0737-4038. doi: 10.1093/oxfordjournals.molbev.a026091.
- Ramesh, P., Lueckmann, J.-M., Boelts, J., Tejero-Cantero, A., Greenberg, D. S., Goncalves, P. J., and Macke, J. H. GATSBI: Generative Adversarial Training for Simulation-Based Inference. In *International Conference on Learning Representations*, October 2021.
- Roset, F. Zuko - Normalizing flows in PyTorch, November 2024.
- Schmitt, M., Bürkner, P.-C., Köthe, U., and Radev, S. T. Detecting Model Misspecification in Amortized Bayesian Inference with Neural Networks: An Extended Investigation, June 2024.
- Tahir, J., Ganguli, S., and Rotskoff, G. M. Features are fate: a theory of transfer learning in high-dimensional regression, October 2024.
- Talts, S., Betancourt, M., Simpson, D., Vehtari, A., and Gelman, A. Validating Bayesian Inference Algorithms with Simulation-Based Calibration, October 2020.
- Tavaré, S., Balding, D. J., Griffiths, R. C., and Donnelly, P. Inferring coalescence times from DNA sequence data. *Genetics*, 145(2):505–518, February 1997. ISSN 0016-6731. doi: 10.1093/genetics/145.2.505.
- Van Geit, W., Gevaert, M., Chindemi, G., Rössert, C., Courcol, J.-D., Muller, E. B., Schürmann, F., Segev, I., and Markram, H. BluePyOpt: Leveraging Open Source Software and Cloud Infrastructure to Optimise Model Parameters in Neuroscience. *Frontiers in Neuroinformatics*, 10, 2016. ISSN 1662-5196.
- Vo, H. D., Fox, Z., Baetica, A., and Munsky, B. Bayesian Estimation for Stochastic Gene Expression Using Multifidelity Models. *The Journal of Physical Chemistry. B*, 123(10):2217–2234, March 2019. ISSN 1520-5207. doi: 10.1021/acs.jpcc.8b10946.
- Vogels, T. P., Sprekeler, H., Zenke, F., Clopath, C., and Gerstner, W. Inhibitory plasticity balances excitation and inhibition in sensory pathways and memory networks. *Science (New York, N.Y.)*, 334(6062):1569–1573, December 2011. ISSN 1095-9203. doi: 10.1126/science.1211095.
- Wang, X., Mak, S., Miller, J., and Wu, J. Local transfer learning Gaussian process modeling, with applications to surrogate modeling of expensive computer simulators, October 2024.
- Ward, D., Cannon, P., Beaumont, M., Fasiolo, M., and Schmon, S. M. Robust Neural Posterior Estimation and Statistical Model Criticism, October 2022.
- Warne, D. J., Prescott, T. P., Baker, R. E., and Simpson, M. J. Multifidelity multilevel Monte Carlo to accelerate approximate Bayesian parameter inference for partially observed stochastic processes. *Journal of Computational Physics*, 469:111543, November 2022. ISSN 00219991. doi: 10.1016/j.jcp.2022.111543.
- Wehenkel, A., Gamella, J. L., Sener, O., Behrmann, J., Sapiro, G., Cuturi, M., and Jacobsen, J.-H. Addressing Misspecification in Simulation-based Inference through Data-driven Calibration, May 2024.
- Zeng, X., Geraci, G., Eldred, M. S., Jakeman, J. D., Gorodetsky, A. A., and Ghanem, R. Multifidelity uncertainty quantification with models based on dissimilar parameters. *Computer Methods in Applied Mechanics and Engineering*, 415:116205, October 2023. ISSN 00457825. doi: 10.1016/j.cma.2023.116205.
- Zenke, F. and Gerstner, W. Limits to high-speed simulations of spiking neural networks using general-purpose computers. *Frontiers in Neuroinformatics*, 8:76, 2014. ISSN 1662-5196. doi: 10.3389/fninf.2014.00076.

A. Further experimental details

A.1. Training procedure

All methods and evaluations were implemented in PyTorch (Paszke et al., 2019). We used Zuko package (Roset, 2024) implementations of Neural Spline flows (NSF) (Durkan et al., 2019) and SBI package (Boelts et al., 2024) for additional functions. The parameters were logit-transformed for numerical stability, and the summary statistics were z-scored to improve the performance of the Normalizing Flows.

The Normalizing Flows had 5 transformations, each parametrized with 50 hidden units and 8 bins, the default settings in the SBI package (Boelts et al., 2024). All results were obtained over an ensemble of 10 networks with a fixed training dataset and a random train-test split.

A.2. Data generation and transformations for increased network performance

During the performance evaluation, we encountered numerical instabilities, particularly with NPE in low-simulation budgets: a substantial proportion of the estimated probability density was placed outside of the uniform prior bounds, a phenomenon dubbed ‘leakage’ that has been previously documented (Greenberg et al., 2019; Deistler et al., 2022). Logit-transforming the model parameters before training the density estimator resolved the issue.

This transformation creates a mapping from a bounded to an unbounded space, resulting in a density estimation within the prior bounds after the inverse transformation. In addition, the summary statistics of the simulations were z-scored for improved performance of the density estimator, the default setting in the SBI package (Boelts et al., 2024).

B. Task 1: Ornstein-Uhlenbeck process

B.1. High-fidelity model: Ornstein-Uhlenbeck Process

The Ornstein-Uhlenbeck process models a drift-diffusion process of a particle starting at position $X(0)$ and drifting towards an equilibrium state. The model has two main components: a *drift* term and a *diffusion* term:

$$dX_t = \underbrace{\gamma(\mu - X_t)dt}_{\text{drift}} + \underbrace{\sigma dW_t}_{\text{diffusion}},$$

where μ is the mean of the asymptotic distribution over positions X , σ is the magnitude of the stochasticity of the process and γ is the convergence speed. $X(0)$ is the initial position of the process, which we assume to be stochastic: $X(0) \sim \mathcal{N}(\mu + \mu_{\text{offset}}, 1)$. The parameters of interest that we aim to estimate are $\mu, \sigma, \gamma, \mu_{\text{offset}}$.

The Ornstein-Uhlenbeck process was approximated with the Euler-Maruyama method:

$$X(t + \delta t) = X(t) + f_{\text{drift}}(t, X) \delta t + f_{\text{diffusion}}(t, X) \sqrt{\delta t} \mathcal{N}(0, 1).$$

Starting from the exact likelihood for the Ornstein-Uhlenbeck process given by Kou et al. (2012):

$$f_{\text{exact hi}}(\mathbf{X} \mid \mu, \gamma, \sigma) = \prod_{t=1}^n \frac{1}{\sqrt{\pi g \sigma}} \exp \left\{ -\frac{1}{g \sigma^2} \left((\mu - X_t) - \sqrt{1 - \gamma g} (\mu - X_{t-1}) \right)^2 \right\},$$

where $g = (1 - \exp(-2\gamma \Delta T))/\gamma$, we modify it by incorporating an additional parameter μ_{offset} to account for a stochastic $X(0)$.

The full likelihood $f_{\text{exact hi}}(\mathbf{X} \mid \mu, \sigma, \gamma, \mu_{\text{offset}})$ is given by

$$f_{\text{exact hi}}(\mathbf{X} \mid \mu, \sigma, \gamma, \mu_{\text{offset}}) = \frac{1}{\sqrt{2\pi}} \exp \left\{ -\frac{(x - (\mu + \mu_{\text{offset}}))^2}{2} \right\} \prod_{t=1}^n \frac{1}{\sqrt{\pi g \sigma}} \exp \left\{ -\frac{1}{g \sigma^2} \left((\mu - X_t) - \sqrt{1 - \gamma g} (\mu - X_{t-1}) \right)^2 \right\}$$

B.2. Low-fidelity model: i.i.d. Gaussian Samples

At convergence, the distribution over X_t approaches a Gaussian distribution with mean μ and standard deviation $\frac{\sigma}{\sqrt{2\gamma}}$. In our setup, we chose a low-fidelity model that corresponds to time-independent random draws from a Gaussian distribution with mean μ_{lo} and standard deviation σ_{lo} :

$$X_t \sim \mathcal{N}(\mu_{\text{lo}}, \sigma_{\text{lo}}^2) \quad (4)$$

The posterior distribution over the parameters of the low-fidelity model has a biased mean influenced by the initial position μ_{offset} and convergence speed γ .

The **summary statistics** from both the high-fidelity and low-fidelity models consisted of 10 subsamples drawn from a trace of 100 timesteps. Parameters and summary statistics are described in Fig. 7.

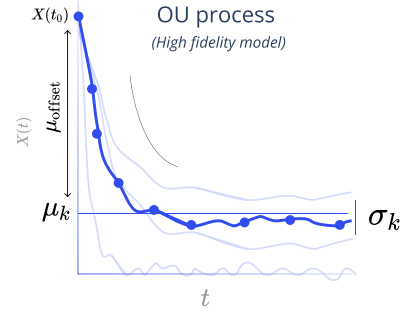


Figure 6. The four parameters of the Ornstein-Uhlenbeck process: the mean μ , standard deviation σ , convergence rate γ , and μ_{offset} , which is the difference between the initial condition $X(0)$ and the mean.

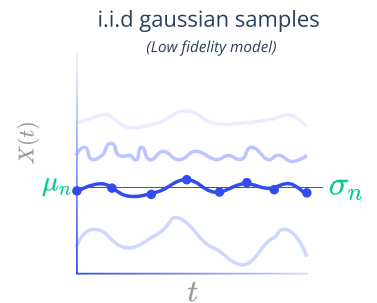


Figure 7. i.i.d. Gaussian samples with mean μ_L and standard deviation σ_L .

B.3. Posterior distribution over different dimensionalities

When the low-fidelity has lower number of parameters than the high-fidelity model, we pre-train the low-fidelity density estimator with dummy parameter values in the dimensions exclusive to the high-fidelity model. Effectively, the pre-conditioning with the dummy variables leads to the pre-trained neural density estimator to effectively estimate the prior distribution over the respective parameters (Figure 8A). Despite the different dimensionalities, the posterior estimates from MF-NPE are closer to the ground-truth posterior than NPE (Figure 8B,C).

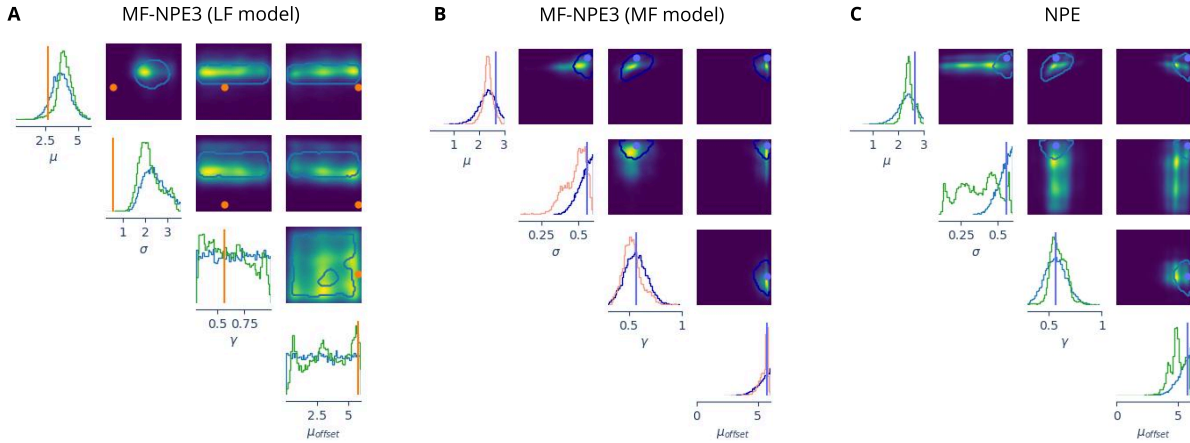


Figure 8. Posterior distributions for the OU process. (A) Posterior distribution under the low-fidelity (i.e., pre-trained) model estimated with MF-NPE. Blue contours contain 68% of the true posterior mass for the low-fidelity model. Vertical bars and dots correspond to the value of the true parameters. Note the different scale in the x-axis with respect to panels (B) and (C). (B) Density estimation with MF-NPE3, after retraining the low-fidelity model on high-fidelity samples. Blue contours contain 68% of the true posterior mass for the high-fidelity model. (C) Density estimation with NPE. Blue contours contain 68% of the true posterior mass for the high-fidelity model.

C. Task 2: Multicompartmental single neuron model

The response of a morphologically detailed neuron to an input current is typically modeled with a multicompartmental neuron model wherein the voltage dynamics of each compartment μ are based on Hodgkin-Huxley equations (Hodgkin & Huxley, 1952):

$$c_m \frac{dV_\mu}{dt} = -i_m^\mu + \frac{I_e^\mu}{A_\mu} + g_{\mu,\mu+1}(V_{\mu+1} - V_\mu) + g_{\mu,\mu-1}(V_{\mu-1} - V_\mu). \quad (5)$$

The total membrane current i_m for a specific compartment is the sum over different types of ion channels i , such as sodium, potassium and leakage channels:

$$i_m = \bar{g}_{Na} m^3 h (V - E_{Na}) + \bar{g}_K n^4 (V - E_K) + \bar{g}_L (V - E_L) + \bar{g}_{MP} (V - E_M) \quad (6)$$

We are interested in inferring the densities of two prominent ion channels \bar{g}_{Na} and \bar{g}_K . The low- and high-fidelity models differ in the number of compartments per branch: the low-fidelity model has a single compartment per branch, while the high-fidelity model consists of eight compartments per branch.

All simulations were performed using Jaxley (Deistler et al., 2024) over 120 ms. The injection current is a step current of 0.55mV over 100 ms, with a delay of 10ms. The step size of the simulator is 0.025.

When sampling from the prior distribution over parameters, approximately 0.1% of the respective simulations had clearly unrealistic summary statistics: these simulations were iteratively replaced by random draws from the prior distribution until we collected a desired number of valid simulations.

C.1. Posterior distributions

Posterior distributions over the parameters of the multicompartmental neuron model trained on 10k high-fidelity simulations.

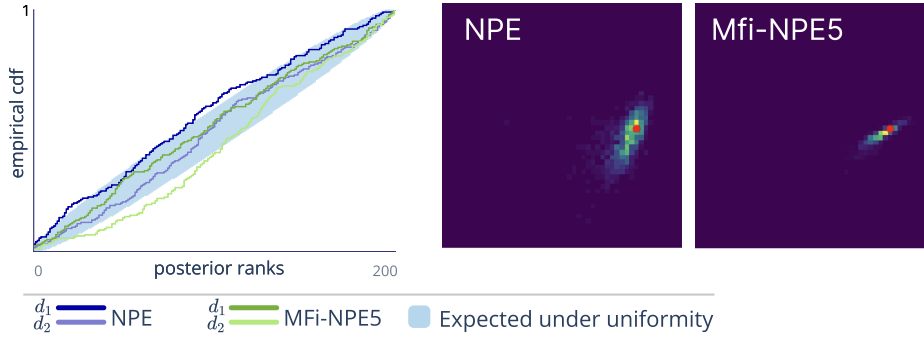


Figure 9. Simulation-based calibration and respective posterior distributions for the multicompartmental neuron model trained on 10k high-fidelity simulations.

C.2. Posterior Predictive Checks

MF-NPE gives similar results as NPE with a training set of high-fidelity simulations up to two orders of magnitude smaller than NPE.

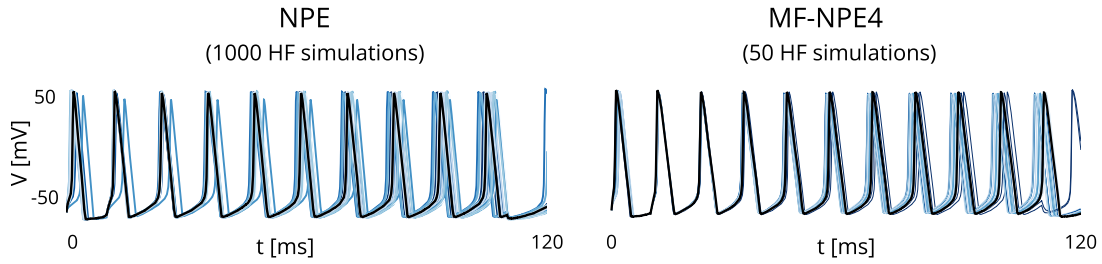


Figure 10. Posterior predictives for the multicompartmental neuron model.

D. Task 3: Spiking network model

D.1. High-fidelity model

We considered a recurrent spiking network of 5120 neurons (4096 excitatory, 1024 inhibitory), with parameters taken from [Confavreux et al. \(2023\)](#). The membrane potential dynamics of neuron j , excitatory (E) or inhibitory (I), followed

$$\tau_m \frac{dV_j}{dt} = -(V_j - V_{\text{rest}}) - g_j^E(t) (V_j - E_E) - g_j^I(t) (V_j - E_I), \quad (7)$$

A postsynaptic spike was generated whenever the membrane potential $V_j(t)$ crossed a threshold $V_j^{\text{th}}(t)$, with an instantaneous reset to V_{reset} . This threshold $V_j^{\text{th}}(t)$ was incremented by $V_{\text{spike}}^{\text{th}}$ every time neuron j spiked and otherwise decayed following

$$\tau_{\text{th}} \frac{dV_j^{\text{th}}}{dt} = V_{\text{base}}^{\text{th}} - V_j^{\text{th}}. \quad (8)$$

The excitatory and inhibitory conductances, g^E and g^I evolved such that

$$g_j^E(t) = a g_j^{\text{AMPA}}(t) + (1-a) g_j^{\text{NMDA}}(t) \quad \text{and} \quad \frac{dg_j^I}{dt} = -\frac{g_j^I}{\tau_{\text{GABA}}} + \sum_{i \in \text{Inh}} w_{ij}(t) \delta_i(t) \quad (9)$$

with $\frac{dg_j^{\text{AMPA}}}{dt} = -\frac{g_j^{\text{AMPA}}}{\tau_{\text{AMPA}}} + \sum_{i \in \text{Exc}} w_{ij}(t) \delta_i(t)$ and $\frac{dg_j^{\text{NMDA}}}{dt} = \frac{g_j^{\text{AMPA}}(t) - g_j^{\text{NMDA}}}{\tau_{\text{NMDA}}}$,

with $w_{ij}(t)$ the connection strength between neurons i and j (unitless), $\delta_k(t) = \sum \delta(t - t_k^*)$ the spike train of pre-synaptic neuron k , where t_k^* denotes the spike times of neuron k , and δ the Dirac delta. All neurons received input from 5k Poisson neurons, with 5% random connectivity and constant rate $r_{\text{ext}} = 10\text{Hz}$ in each simulation. The recurrent connectivity was instantiated with random sparse connectivity (10%). All recurrent synapses in the network (E -to- E and E -to- I , I -to- E , I -to- I) underwent variations of spike-timing dependent plasticity (STDP) ([Gerstner & Kistler, 2002](#); [Confavreux et al., 2023](#)). Given the learning rate η , the weights between the neurons i and j of connection type X -to- Y evolved over time as:

$$\frac{dw_{ij}}{dt} = \eta [\delta_{\text{pre}}(t) (\alpha + \kappa x_{\text{post}}(t)) + \delta_{\text{post}}(t) (\beta + \gamma x_{\text{pre}}(t))]. \quad (10)$$

with variables $x_i(t)$ and $x_j(t)$ describing the pre- and postsynaptic spikes over time:

$$\frac{dx_i}{dt} = -\frac{x_i}{\tau_{XY}^{\text{pre}}} + \delta_i(t) \quad \text{and} \quad \frac{dx_j}{dt} = -\frac{x_j}{\tau_{XY}^{\text{post}}} + \delta_j(t) \quad (11)$$

with τ_{XY}^{pre} and τ_{XY}^{post} the time constants of the traces associated with the pre- and postsynaptic neurons, respectively.

The 24 free parameters of interest were $\tau_{\text{pre}}, \tau_{\text{post}}, \alpha, \beta, \kappa, \gamma$ multiplied by the number of synapse types (e.g., $\alpha_{EE}, \alpha_{II}, \alpha_{EI}, \alpha_{IE}$), following previous work ([Confavreux et al., 2023](#)).

D.2. Low-fidelity model

Following previous work ([Confavreux et al., 2023](#); [Vogels et al., 2011](#); [Dayan & Abbott, 2001](#)), a (partial) mean-field theory applied to the E -to- E and E -to- I connections in the model described above gave:

$$r_E^* = \frac{-\alpha_{EE} - \beta_{EE}}{\lambda_{EE}} \quad \text{and} \quad r_I^* = \frac{-\alpha_{EI} r_E^*}{\beta_{EI} + \lambda_{EI} r_E^*} \quad (12)$$

with r_E^* and r_I^* the firing rates of the excitatory (resp. inhibitory) population at steady state, and

$$\lambda_{XY} = \kappa_{XY} \tau_{XY}^{\text{post}} + \gamma_{XY}^{\text{pre}} \quad (13)$$

With type $(X, Y) \in \{E, I\}$. For all synapse types, we assume $(-\alpha_{XY} - \beta_{XY}) > 0$ and $\lambda_{XY} > 0$, as a second-order stability condition ([Confavreux et al., 2023](#)). Note that in this low-fidelity model, we only considered 2 of the 4 plastic conditions, and thus 12 of the 24 free parameters of the high-fidelity model.

E. Prior bounds across tasks

For the OU process task, we chose a uniform prior with bounds that would lead to a range of different outputs. For the multicompartment neuron model task, we chose a uniform prior with bounds based on the work of [Deistler et al. \(2022\)](#). For the spiking network model task, we chose a uniform prior with bounds based on the work of [Confavreux et al. \(2023\)](#).

Table 2. Prior bounds for i.i.d. Gaussian samples and the Ornstein-Uhlenbeck process.

PARAMETER NAME	LOWER BOUND	UPPER BOUND
μ	0.1	3.0
σ	0.1	0.6
γ	0.1	1.0
μ_{offset}	0.0	4.0

Table 3. Prior bounds for the single- and multicompartmental neuron model.

PARAMETER NAME	LOWER BOUND	UPPER BOUND
\bar{g}_{NA}	0.005	0.8
\bar{g}_{K}	10^{-6}	0.15

Table 4. Prior bounds for each synapse type (E -to- E , E -to- I , I -to- E and I -to- I) for the spiking neural network and mean-field model.

PARAMETER NAME	LOWER BOUND	UPPER BOUND
τ_{pre}	0.01	0.1
τ_{post}	0.01	0.1
α	-2	2
β	-2	2
γ	-2	2
κ	-2	2

F. Sequential Algorithms

F.1. MF-TSNPE

Algorithm 2 MF-TSNPE

Input: N pairs of $(\boldsymbol{\theta}, \mathbf{x}_L)$; conditional density estimators $q_\psi(\boldsymbol{\theta}|\mathbf{x}_L)$ and $q_\phi(\boldsymbol{\theta}|\mathbf{x})$ with learnable parameters ψ and ϕ ; early stopping criterion S ; simulator $p_H(\mathbf{x}|\boldsymbol{\theta})$; prior $p(\boldsymbol{\theta})$; number of rounds R ; ϵ that defines the highest-probability region (HPR_ϵ); number of high-fidelity simulations per round M .

Output: posterior estimate $q_\phi(\boldsymbol{\theta}|\mathbf{x})$

$$\mathcal{L}(\psi) = \frac{1}{N} \sum_{i=1}^N -\log q_\psi(\boldsymbol{\theta}_i|\mathbf{x}_i^L).$$

for epoch in epochs **do**

train q_ψ to minimize $\mathcal{L}(\psi)$ until S is reached.

end for

Initialize $\tilde{p}(\boldsymbol{\theta})$ as $p(\boldsymbol{\theta})$

Initialize q_ϕ with weights and biases of trained q_ψ .

for r in R **do**

$\boldsymbol{\theta}^{(r)} \sim \tilde{p}(\boldsymbol{\theta})$, sample parameters from proposal

$\mathbf{x}^{(r)} \sim p_H(\mathbf{x}|\boldsymbol{\theta}^{(r)})$, generate high-fidelity simulations

for epoch in epochs **do**

$$\mathcal{L}(\phi) = \frac{1}{M} \sum_{i=1}^M -\log q_\phi(\boldsymbol{\theta}_i^{(r)}|\mathbf{x}_i^{(r)}).$$

train q_ϕ to minimize $\mathcal{L}(\phi)$ until S is reached.

end for

Compute expected coverage $(\tilde{p}(\boldsymbol{\theta}), q_\phi)$

$$\tilde{p}(\boldsymbol{\theta}) \propto p(\boldsymbol{\theta}) \cdot \mathbb{1}_{\boldsymbol{\theta} \in \text{HPR}_\epsilon}$$

end for

All experiments were ran with $R = 5$ rounds and $\epsilon = 1e^{-6}$. More details about TSNPE at [Deistler et al. \(2022\)](#).

F.2. A-MF-TSNPE

Algorithm 3 A-MF-TSNPE

Input: N pairs of $(\boldsymbol{\theta}, \mathbf{x}_L)$; conditional density estimator $q_\psi(\boldsymbol{\theta}|\mathbf{x}_L)$ with learnable parameters ψ and an ensemble of conditional density estimators $\{q_\phi^e(\boldsymbol{\theta}|\mathbf{x})\}_E^e$, each with independent ϕ ; early stopping criterion S ; simulator $p_H(\mathbf{x}|\boldsymbol{\theta})$; prior $p(\boldsymbol{\theta})$; number of rounds R ; ϵ that defines the highest-probability region (HPR_ϵ); number of high-fidelity simulations per round M .

Output: Ensemble posterior estimate $q_\phi(\boldsymbol{\theta}|\mathbf{x}) = \frac{1}{E} \sum_{e=1}^E q_\phi^e(\boldsymbol{\theta}|\mathbf{x})$

$\mathcal{L}(\psi) = \frac{1}{N} \sum_{i=1}^N -\log q_\psi(\boldsymbol{\theta}_i|\mathbf{x}_i^L)$.

for epoch in epochs **do**

 train q_ψ to minimize $\mathcal{L}(\psi)$ until S is reached.

end for

for $e \in \text{Ensemble}$ **do**

 Initialize q_ϕ^e with weights and biases of trained q_ψ .

end for

$\boldsymbol{\theta}_{\text{pool}} \sim p(\boldsymbol{\theta})$

Initialize $\tilde{p}(\boldsymbol{\theta})$ as $p(\boldsymbol{\theta})$

for r in R **do**

$\boldsymbol{\theta}_{\text{prop}}^{(r)} \sim \tilde{p}(\boldsymbol{\theta})$, generate $M - B$ samples from proposal

$\boldsymbol{\theta}_{\text{active}}^{(r)} = \text{top } B \text{ values from } \boldsymbol{\theta}_{\text{pool}} \text{ using the acquisition function eq. (2)}$

$\boldsymbol{\theta}^{(r)} = \{\boldsymbol{\theta}_{\text{prop}}^{(r)} \cup \boldsymbol{\theta}_{\text{active}}^{(r)}\}$

$\mathbf{x}^{(r)} \sim p_H(\mathbf{x}|\boldsymbol{\theta}^{(r)})$, generate high-fidelity simulations

for $e \in \text{Ensemble}$ **do**

for epoch in epochs **do**

$\mathcal{L}(\phi) = \frac{1}{M} \sum_{i=1}^M -\log q_\phi^e(\boldsymbol{\theta}_i^{(r)}|\mathbf{x}_i^{(r)})$.

 train q_ϕ to minimize $\mathcal{L}(\phi)$ until S is reached.

end for

end for

 Compute expected coverage $(\tilde{p}(\boldsymbol{\theta}), \frac{1}{E} \sum q_\phi^e(\boldsymbol{\theta}|\mathbf{x}))$

$\tilde{p}(\boldsymbol{\theta}) \propto p(\boldsymbol{\theta}) \cdot \mathbb{1}_{\boldsymbol{\theta} \in \text{HPR}_\epsilon}$

end for

All experiments were ran with $R = 5$ rounds, $\epsilon = 1e^{-6}$, and an ensemble of 5 networks. We set $B = .2M$ to mitigate the concern of biasing the posterior with parameters selected with the acquisition function.